Shock Waves (2001) 10: 395–404

Shock Waves

Investigations of gas and particle dynamics in first generation needle-free drug delivery devices

N.J. Quinlan[1,*], M.A.F. Kendall[1], B.J. Bellhouse[1], R.W. Ainsworth[2]

[1] PowderJect Centre for Gene and Drug Delivery Research, University of Oxford, Oxford OX2 6PE, UK
[2] Department of Engineering Science, University of Oxford, Oxford OX1 3PJ, UK

Received 12 March 2000 / Accepted 8 June 2000

Abstract. Transdermal powdered drug delivery involves the propulsion of solid drug particles into the skin by means of high-speed gas-particle flow. The fluid dynamics of this technology have been investigated in devices consisting of a convergent-divergent nozzle located downstream of a bursting membrane, which serves both to initiate gas flow (functioning as the diaphragm of a shock tube) and to retain the drug particles before actuation. Pressure surveys of flow in devices with contoured nozzles of relatively low exit-to-throat area ratio and a conical nozzle of higher area ratio have indicated a starting process of approximately 200 μs typical duration, followed by a quasi-steady supersonic flow. The velocity of drug particles exiting the contoured nozzles was measured at up to 1050 m/s, indicating that particle acceleration took place primarily in the quasi-steady flow. In the conical nozzle, which had larger exit area ratio, the quasi-steady nozzle flow was found to be overexpanded, resulting in a shock system within the nozzle. Particles were typically delivered by these nozzles at 400 m/s, suggesting that the starting process and the quasi-steady shock processed flow are both responsible for acceleration of the particle payload. The larger exit area of the conical nozzle tested enables drug delivery over a larger target disc, which may be advantageous.

Key words: Needle-free drug delivery, Transdermal powdered drug delivery, Powder injection, Biolistics, Supersonic nozzle, Shock tube, Doppler global velocimetry

1 Introduction

Over the past five years, a new technology for the needle-free injection of drugs into the skin has emerged. The underlying principle is to accelerate powdered drug particles to an appropriate velocity in a gas jet, directed towards the skin, such that they can pass through the outer skin and lodge in deeper layers of tissue without causing injury or pain. This technology, known generically as transdermal powdered drug delivery, was first patented by Bellhouse et al. (1994) and is being developed commercially as the PowderJect system. It has been shown to be a viable alternative to injection by needle and syringe for many applications (Burkoth et al. 1999). Moreover, it can enhance the potential of a variety of drugs and vaccines which is limited by available delivery methods.

Transdermal powder drug delivery has many advantages over other techniques. Most obviously, it is painless and causes no injury, unlike liquid jet injectors and the conventional needle and syringe. It does not leave dangerous sharps for disposal, create a contamination hazard, or require a skilled operator. It shares some of the advantages of the needle and syringe in offering rapid action and localised delivery, when required. The direct use of drugs in powder (rather than liquid) form is attractive in itself, since drugs are often manufactured and distributed as powder for compact storage and improved chemical stability, and must be constituted as a liquid prior to use in a needle and syringe. In addition to these logistical advantages, this drug delivery technique can enhance the power of certain new and existing treatments. DNA vaccines, for example, as well as some conventional vaccines and anti-viral drugs, benefit from delivery to particular layers within the skin, which is difficult to achieve accurately with conventional technology. The PowderJect system offers the potential to target these specific layers through control of drug particle kinetic energy (and hence, penetration depth), or at least to achieve blanket delivery into the shallow regions of the skin. Drugs which require self-administration, or local delivery to sensitive sites, can be made more attractive and accessible for the patient with this technology.

Successful implementation of this simple concept is not trivial. In order to achieve an optimal biological response, it is desirable to deliver the drug particle payload

Correspondence to: Nathan J. Quinlan
* *Present address:* Department of Mechanical Engineering, National University of Ireland, Galway, Ireland
(e-mail: nathan.quinlan@nuigalway.ie)

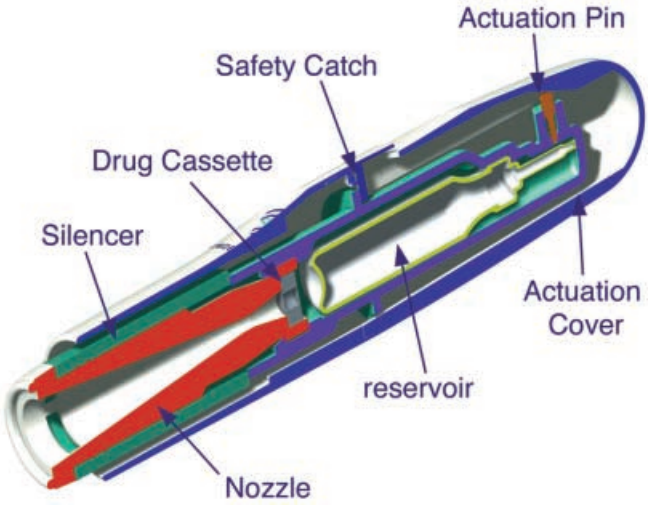

Fig. 1. Outline diagram of a prototype PowderJect device with a conical divergent nozzle

with uniform velocity and particle number density over the largest possible area. This capability must be available in an economical, compact (hand-held), robust and acoustically quiet system. Future applications of the technology may call for devices with adjustable performance in order to accommodate a variety of drugs and doses. These criteria demand a thorough fundamental understanding of physical and biological processes underlying transdermal powdered drug particle delivery. A substantial multidisciplinary programme of research has been directed towards this goal.

An integrated review of the medical, pharmacological and engineering aspects of the technology has been given by Burkoth et al. (1999). The paper includes descriptions of clinical trials in which efficacious delivery was achieved for lidocaine, a local anaesthetic, and encouraging results were obtained for alprostadil, which is used in the treatment of male erectile dysfunction. Recently, Kendall et al. (2000) have described fundamental investigations of the biomechanics of powder injection, using a calibrated piston-based test system to propel particles into excised skin at known velocities up to 260 m/s. It was demonstrated in these experiments that particles can penetrate the stratum corneum (the tough outermost layer of the skin) to reach underlying tissue, and the dependence of penetration depth on particle velocity, size and density was characterised.

This interaction between high-velocity drug particles and biological tissue is one essential facet of the complete powder injection system. The means of imparting momentum to the powdered drug dose is equally important. In the practical drug delivery devices to be discussed here, particles are accelerated by entrainment in a high-speed gas flow. Particular aspects of the fluid dynamics of certain devices have been discussed by Bellhouse et al. (1997) and Quinlan et al. (1997). The present paper is an integrated account of research into the fluid dynamics of early generations of prototype practical dermal PowderJect devices in which gas-particle flows are exploited to realise the concept of high-velocity particle injection.

The overall objective of this research is to arrive at an understanding of the mechanisms which determine the distribution and velocities of drug particles accelerated through these prototype drug delivery devices. Particle velocity and distribution (along with the mechanical properties of particles and skin) are fundamentally important characteristics which determine the efficacy of drug delivery. In order to explore the fluid dynamics which underlie these aspects of device performance, prototype devices were characterised experimentally by pressure surveys and field measurements of time-integrated particle velocity. Analytical modelling of bulk gas flows in the devices has also been carried out. This research has been concerned with three prototype device nozzles, which will be discussed in detail below.

2 Prototype devices tested

The configuration of a clinical device for transdermal powdered drug delivery is shown in Fig. 1. The key components of the device are a gas reservoir, in which compressed helium is stored, typically at a pressure of tens of atmospheres; a drug cassette, in which the powdered drug is retained between a pair of bursting membranes; and a convergent-divergent nozzle. Basic compressible flow theory provides a qualitative description of this system's expected mode of operation. When gas is released from the reservoir, a large pressure difference builds up across the drug cassette. The membranes rupture, leading to the formation of a shock wave, which propagates down the nozzle and initiates an unsteady high-speed gas flow, as in a classical shock tube. Later, a sustained bulk flow of gas from the cylinder is established, and under certain conditions, the device's convergent-divergent nozzle functions as a supersonic nozzle. In the course of these processes, particles are entrained in the gas flow and accelerate towards the nozzle exit. As the particle-laden flow impinges on the skin, gas is deflected away to the side and vents to the atmosphere through a silencer. The particles, with their relatively large inertia, maintain a high axial velocity and penetrate the tough outer layer of dead cells (the stratum corneum), coming to rest in deeper layers of the skin. There, the drug either acts locally, or diffuses into the bloodstream for systemic effect.

The configuration of the prototype devices tested here is illustrated in Fig. 2. In contrast with the production design shown in Fig. 1, these prototypes feature an annular valve at the downstream end of the cylindrical reservoir, connecting the reservoir to the rupture chamber. The prototypes were tested without a silencer for the purposes of this investigation. Devices were tested with two contoured nozzles, which differed in their nominal exit Mach numbers, and a conical nozzle, with a substantially larger exit area.

A geometric description of each nozzle is given in Table 1. Some nozzle flow parameters, calculated for steady quasi-one-dimensional isentropic flow, are also included to

Table 1. Geometric parameters and idealised flow parameters for the two contoured nozzles and one conical nozzle tested (MOC: Method Of Characteristics)

Nozzle designation		Mach 2.5 contoured	Mach 3.5 contoured	Conical
Geometry	Divergent section	MOC design	MOC design	Conical
	Exit-to-throat area ratio	2.21	4.27	20.3
Isentropic supersonic	Exit Mach number	2.54	3.53	6.52
exit flow conditions	Exit velocity (m/s)	1450	1580	1700
Minimum ratio of total	Choking at throat	1.06	1.02	1.00
pressure to back pressure for	Supersonic exit flow	2.20	3.96	17.3

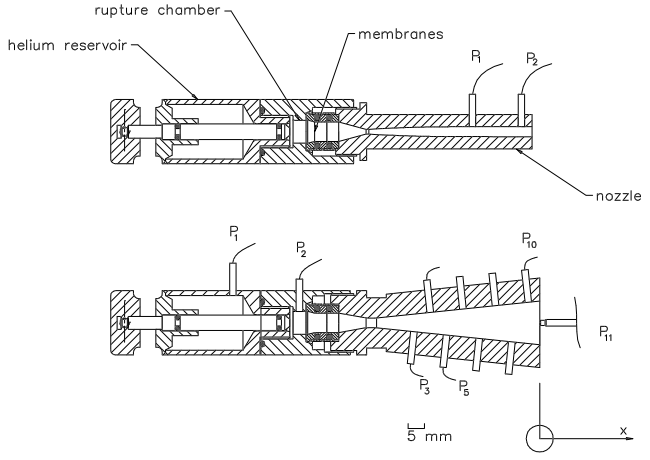

Fig. 2. Section diagrams of the test devices with pressure transducer instrumentation. Contoured nozzle and conical nozzle devices are shown in the upper and lower diagrams, respectively

illustrate the relationship between device geometry and performance. As the figures in Table 1 suggest, the large diameter conical nozzle will require considerably higher operating pressure ratios to avoid overexpanded flow. Consequently, the larger footprint area achieved with the conical nozzle is accompanied by a reduction in gas exit velocities.

3 Experimental and analytical methods

The unsteady gas flow field in one of the contoured nozzles, and in the conical nozzle, was investigated using fast-response pressure transducers. In the Mach 3.5 contoured nozzle, static pressure measurements were made at two locations. More extensive pressure measurements were carried out in the conical nozzle – static and Pitot pressure measurements were made at a total of eight locations in the divergent section, and static pressure was also measured in the rupture chamber. These measurements of rupture chamber pressure were compared with a simple analytical model of the blowdown process. The particle velocity field, which is ultimately the most important mechanical operating characteristic of the device, was measured using Doppler Global Velocimetry (DGV) in the jets generated by a contoured and a conical nozzle. These various techniques are explained more fully below.

3.1 Gas dynamics instrumentation

Various Kulite type XCQ semiconductor absolute pressure transducers (Kulite Semiconductor Products Inc., One Willow Tree Road, Leonia, NJ 07605, USA) were used for measurements of unsteady pressure in both types of drug delivery nozzle. These transducers satisfied the need for compact fast-response instrumentation to record the unsteady short-duration flow in the nozzle. Each transducer was installed with an elastomeric RTV coating to protect the sensor and to damp resonant oscillations. The resonant frequency of these transducers is of the order of 400 kHz or higher.

Two such transducers were flush mounted in the interior wall of the Mach 3.5 contoured nozzle at positions 3.25 and 18.25 mm upstream of the nozzle exit, as shown in Fig. 2. Pressure measurements in the conical nozzle were more extensive. In the divergent part of this nozzle, static pressure was measured at a range of axial positions using Kulite transducers. They were flush-mounted in the nozzle wall at 5 mm intervals from 3.5 mm to 38.5 mm upstream of the exit plane. Up to four transducers were used in each individual experiment, while blanking plugs were inserted in the remaining transducer mounting ports. At the same time, a PCB 111A26 piezoelectric pressure transducer (PCB Piezotronics Inc., 3425 Walden Ave., Depew, NY 14043-2495, USA) was used to measure static pressure in the rupture chamber. This transucer has a specified rise time of less than 1 μs and a natural frequency in excess of 500 kHz.

In addition to the static pressure measurements, a Pitot probe (designated P_{11} in Fig. 2) was mounted perpendicular to the exit plane of the conical nozzle. The probe consisted of a Kulite XCQ pressure transducer mounted in a stainless steel casing of outer diameter 2 mm. The probe was stepped along the nozzle centreline in 5 mm increments between successive experiments. The wall-mounted static transducers were arranged so that a Pitot measurement was always taken in conjunction with a wall static pressure measurement at the same axial station. The ratio of Pitot to static pressure was then used to obtain the time history of flow Mach number for each run, using the Pitot-Rayleigh relation. Wall static pressure measurements were repeated without the Pitot probe

to determine the effect of the probe on the static pressure in the flow. It was found that the probe had no detectable effect at positions up to 23.5 mm upstream of the nozzle exit plane. The arrangement of Pitot and static transducers was assessed in shock tube tests, and yielded results within 2% of ideal theory.

3.2 Analytical modelling

A simple mathematical model of the process of reservoir drainage was derived, with the aim of predicting the variation in time of pressure and temperature in both the reservoir and the rupture chamber. The model, which is explained in full by Quinlan (1999), is based on the following simplifications. Flow from the reservoir into the rupture chamber, and from the rupture chamber through the nozzle throat, is assumed to be steady. The gas within each chamber is assumed to be stagnant and uniform, undergoing isentropic changes of state as it expands or is compressed. The mass flow from the reservoir through the narrow annular valve into the rupture chamber is modified by an empirically determined discharge coefficient. Heat transfer from the device walls to the gas in this valve is expected to be significant. It is represented approximately in the model by the assumption that inflowing gas stagnates in the rupture chamber at ambient temperature and reaches thermal equilibrium with the contents of the chamber.

Under the assumption of stagnation in the rupture chamber, the temperature and pressure of gas in that chamber are identical to the total pressure and total temperature for flow through the nozzle. This is the main motivation for this modelling work.

These assumptions lead to a model which can be reduced to two ordinary differential equations describing the variation of pressure in each chamber. These equations are solved by a simple numerical time-marching method. Simple treatments of the early strongly unsteady flow following membrane rupture are also incorporated. However, it must be emphasised that the validity of the analysis is restricted to the later quasi-steady stages of flow. The model was implemented for both contoured and conical nozzles.

3.3 Particle dynamics measurements

Doppler Global Velocimetry was used to measure the velocity of drug particles delivered by the devices. DGV is an emerging optical technique for fluid dynamics measurements which yields a velocity distribution over a two-dimensional planar measurement region. It is essentially a spectroscopic imaging technique, and may be implemented with continuous laser illumination (for time-integrated measurements) or single illumination pulses (for near-instantaneous measurement in unsteady flows). Overviews of the evolution of DGV and the current state of the art have been published by Meyers (1995) and Ainsworth et al. (1997). The Oxford implementation of the DGV principle, and its application to drug delivery

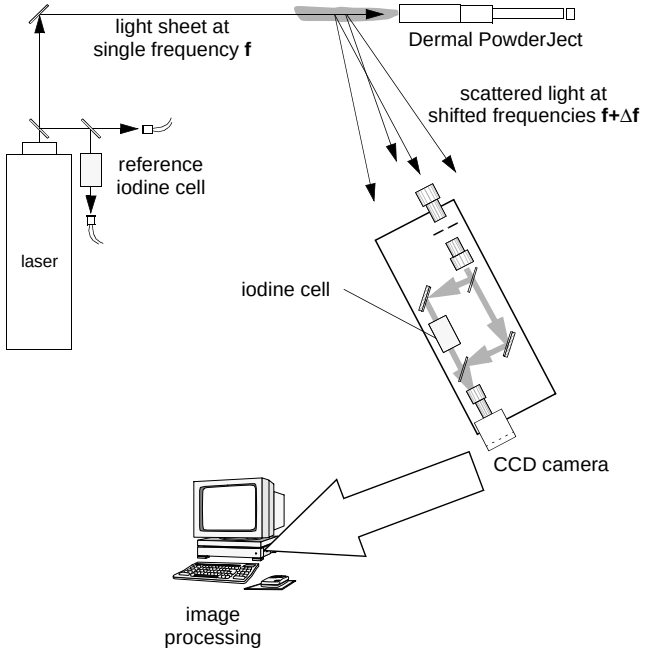

Fig. 3. A schematic diagram of the Oxford DGV apparatus (not to scale), as arranged in experiments on drug delivery devices. The light sheet lies in a plane normal to that of the diagram

devices, are described in detail by Thorpe et al. (1996) and Quinlan et al. (1997), respectively.

The Oxford DGV apparatus, as configured in this application, is outlined in Fig. 3. A line-narrowed Argon ion continuous-wave laser illuminates a planar measurement region in the flow-field. Doppler-shifted light scattered by particles which pass through the measurement plane is gathered by the imaging system, in which it is manipulated to form twin images of the flow-field on a charge-coupled device (CCD) camera. The light which forms one of the images passes through a cell filled with iodine vapour. The frequency of the illuminating laser radiation is tuned onto an absorption feature of iodine, so that light absorption in the iodine cell is a strong function of light frequency over the bandwidth (typically of the order of 1 GHz) of the absorption feature. The absorption profile of the iodine cell is calibrated and used to determine Doppler frequency shift and hence velocity. A second flow-field image, unprocessed by the iodine cell, is required to decouple the filtering action of the iodine vapour from other influences on image intensity (such as non-uniformity in illumination and particle number density).

In this study, DGV was used to measure the velocity of model drug particles emerging from prototype PowderJect drug delivery devices. In each experiment, a device was loaded with particles and fired into free air, generating a two-phase jet. The measurement region was illuminated continuously, and the CCD camera was exposed for 1 to 2 seconds, a period many times longer than the duration of the flow. As a result, the velocity measurement is not time-resolved, but is representative of the velocities of all particles which pass through each point, with a bias to-

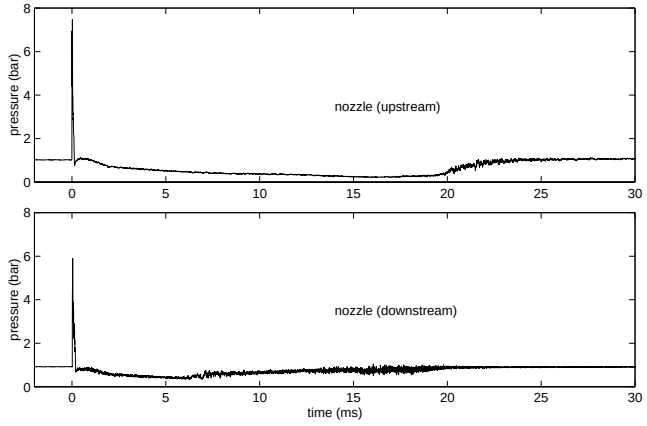

Fig. 4. Measured pressure histories in the Mach 3.5 contoured nozzle, with 12 μm Mylar membranes, over the duration of a complete run

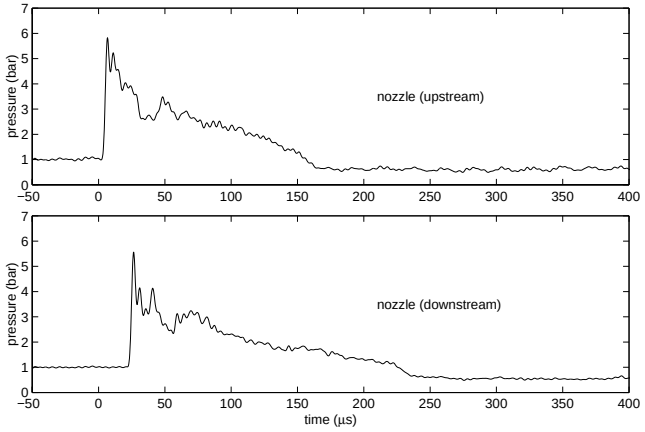

Fig. 5. Measured pressure histories for the early stages of flow in the Mach 3.5 contoured nozzle, with 23 μm Mylar membranes

wards the slower particles and those which scatter most light.

The experiment was configured for measurement of axial velocity in a plane containing the nozzle axis. The measurement region extended from approximately 3 mm to a maximum of 35 mm downstream of the nozzle exit, and was wide enough to accommodate the full diameter of the jet.

The particles used in velocimetry test payloads were polymer microspheres (Duke Scientific, PO Box 50005, Palo Alto, California 94303, USA), which were chosen to emulate the physical properties of drug particles, while providing more consistency in particle size. Microsphere payloads of mean diameter 4.7 μm, 15.5 μm and 26.1 μm were used, with a maximum standard deviation of 13% of the mean size. The density of the particle material is 1050 kg/m^3. Payload masses of 1, 3 and 5 mg were tested.

4 Results

4.1 Gas dynamics: contoured nozzle

The Mach 3.5 contoured nozzle provided a flow which could be explained, with some success, in terms of classical unsteady and steady flow phenomena. In Fig. 4, the pressure histories for both nozzle-mounted transducers, over the duration of a complete run, are shown. The initial transient gives way, in under 1 ms, to a slowly varying state at a pressure below atmospheric pressure. This indicates a quasi-steady overexpanded supersonic flow, with one or more shock waves positioned downstream of the measurement locations. Pressure falls with the decay in total pressure due to drainage of gas from the reservoir system. Around 6 ms after the beginning of flow, pressure begins to rise slowly at the downstream transducer, as a shock or a system of shocks travels up the nozzle. These shocks are detected later at the upstream transducer. The greater level of rapid pressure fluctuations at the downstream transducer is probably due to its proximity to the exit and to the higher local boundary layer thickness.

These results establish the basic picture of flow in the device, in which a classical shock tube flow is followed by a blowdown flow which varies slowly enough to exhibit the properties of a steady supersonic nozzle flow. A short-lived starting process effects the transition between the two classical flow regimes.

Flow reproducibility was assessed in the Mach 3.5 contoured nozzle over five experiments under nominally identical conditions. Variability of approximately ± 2 ms was observed in the timing of the passage of the quasi-steady shock system through the nozzle. At other stages of the flow, measured pressure deviated by less than ± 0.14 bar from the mean over all five experiments.

Measurements of pressure over the first 0.5 ms of flow are shown in detail in Fig. 5. The primary starting shock is followed by a complex starting process, after which the slowly varying supersonic flow is established. In particular, the pressure decrease which precedes the slowly varying flow may be the signature of a secondary shock wave (as described by Smith (1966) and Amman (1969), among others), which travels upstream with respect to the gas, but is swept downstream in the reference frame of the nozzle. The longer duration of the starting process at the downstream transducer supports this interpretation of the results. The expansion wave generated by the bursting of the membranes, having reflected off the upstream wall of the rupture chamber and followed the primary shock downstream, may also be a significant element of the starting process. The primary shock decays in transit between the transducers, due to viscous attenuation, increase in duct area, and interaction with the reflected expansion wave. Its average propagation speed has been measured as 844 m/s, which corresponds to a gas velocity of 586 m/s immediately behind the shock.

4.2 Gas dynamics: conical nozzle

In Fig. 6, pressure measurements taken in the reservoir, rupture chamber and nozzle transducers are shown, along with computed pressure histories for the reservoir and rup-

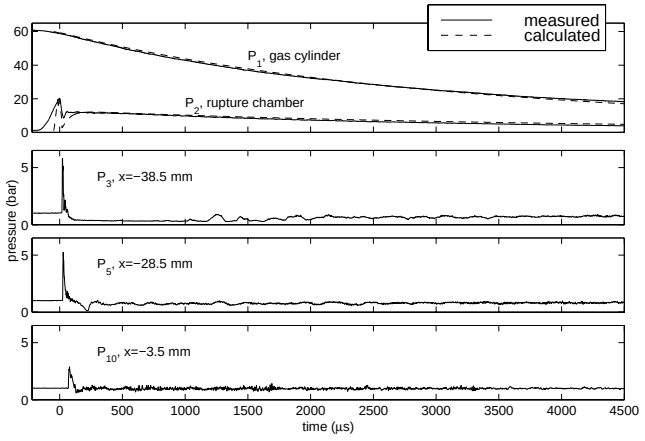

Fig. 6. Measured pressures in the cylinder, rupture chamber and nozzle for a device with a conical nozzle, with computations of pressure in the cylinder and rupture chamber. Transducer locations are specified with respect to the nozzle exit

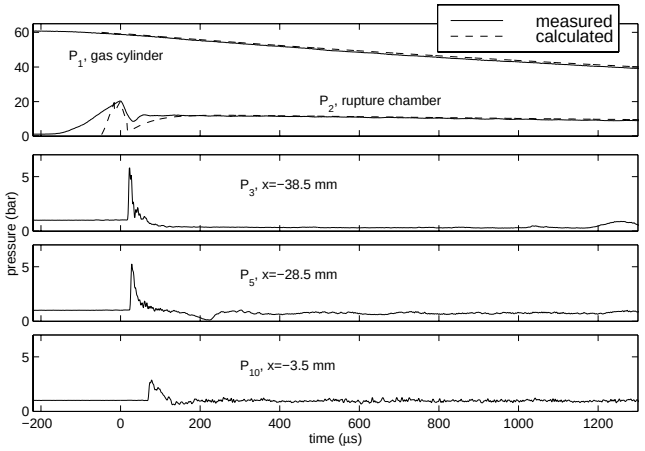

Fig. 7. Measured and computed pressure in the cylinder and rupture chamber, and measured pressures in the nozzle, during the early stages of operation with a conical nozzle. Transducer locations are specified with respect to the nozzle exit

ture chamber, for a device fitted with a conical nozzle. Computations and measurements for the early stages of a run are shown in Fig. 7. In the reservoir, pressure begins to decay monotonically when the valve is opened, and asymptotically approaches one atmosphere. In the rupture chamber, the bursting of each membrane is signalled by a sharp drop in pressure as an expansion wave passes over the transducer. After the downstream membrane bursts, rupture chamber pressure rises slightly before beginning to decay relatively slowly.

Membrane rupture generates a shock which propagates through the nozzle, decelerating to a velocity of approximately 610 m/s at the exit plane. This primary shock initiates a complex starting process, involving an expansion to below atmospheric pressure (at 220 μs on transducer P_5, and 130 μs on P_{10}, as shown in Fig. 7) followed by recompression to a level just below atmospheric pressure. Pressure then fluctuates between 0.8 and 1 bar, finally returning to atmospheric pressure.

According to the nozzle parameters in Table 1, if the rupture chamber static pressure is assumed equal to the nozzle total pressure, supersonic flow can be sustained at the exit only while the rupture chamber pressure exceeds 17.3 atmospheres. At this critical pressure level, supersonic flow will terminate in a shock at the nozzle exit. The measured rupture chamber pressure, however, falls below this level before any gas flow is sensed at the nozzle transducers. As a result, quasi-steady supersonic nozzle flow does not extend to the nozzle exit plane. It is terminated by a shock front which is generated at the nozzle exit to compress the exit flow to atmospheric pressure, and is swept upstream during the starting process at approximately 300 m/s (in the laboratory frame of reference). The shock front later becomes quasi-stationary, moving slowly upstream as the total pressure (measured in the device rupture chamber) decays.

The effect of the shock front on the nozzle flow is illustrated by the axial Mach number profiles measured at various times, shown in Fig. 8. The theoretical profile for isentropic quasi-one-dimensional flow is also shown. Consider the Mach number profiles measured at times 500 μs and 1000 μs after membrane rupture. At 38.5 mm upstream of the exit, the experimental data and isentropic theory are in good agreement at $M = 3$. Further downstream, however, measurements and theory diverge. For instance, measured Mach numbers gradually decrease from approximately 2.5 (23.5 mm upstream of the exit plane) to 1.5 (at the exit), whereas the isentropic Mach numbers at these positions are 4.5 and 6.5 respectively. The Mach number measurement 38.5 mm upstream of the exit 2000 μs after rupture is no longer consistent with isentropic theory, while the Mach number values further downstream are falling. This trend continues for the remainder of the flow. The gradual decay in Mach number through supersonic values along the length of the nozzle indicates that the shock front is very likely oblique. This theory is further supported by the relatively small drop (by a factor of approximately 2) in total pressure across the shock front.

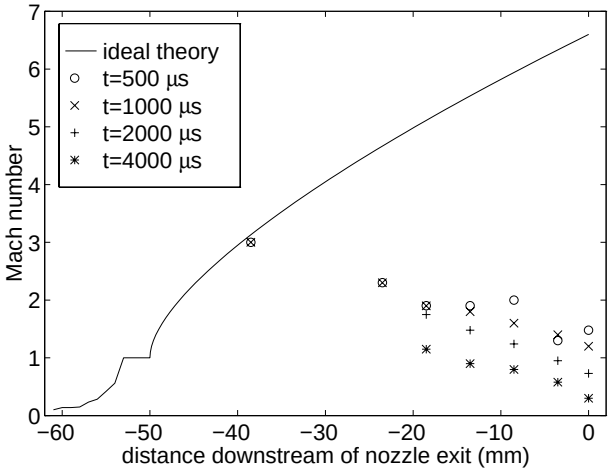

Fig. 8. Experimental and ideal axial Mach number within the PowderJect conical nozzle

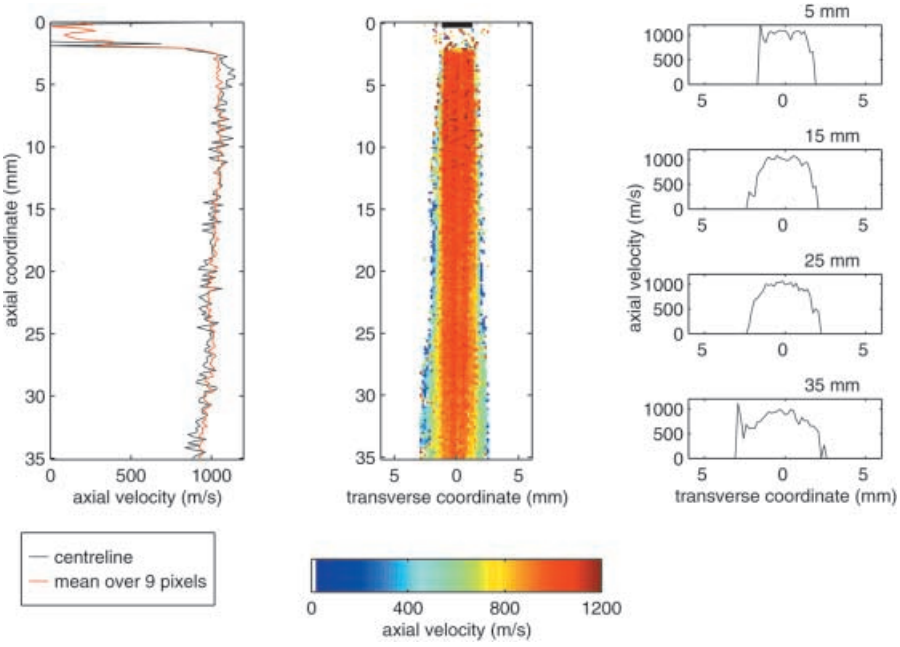

Fig. 9. A colourmap representation of the axial velocity field, an axial profile on the centreline, and profiles at various transverse sections, measured for a payload of 1.0 mg of 4.7 μm polymer microspheres, delivered from a device with a Mach 2.5 contoured nozzle. The bar at the top of the image indicates the position and diameter of the nozzle exit

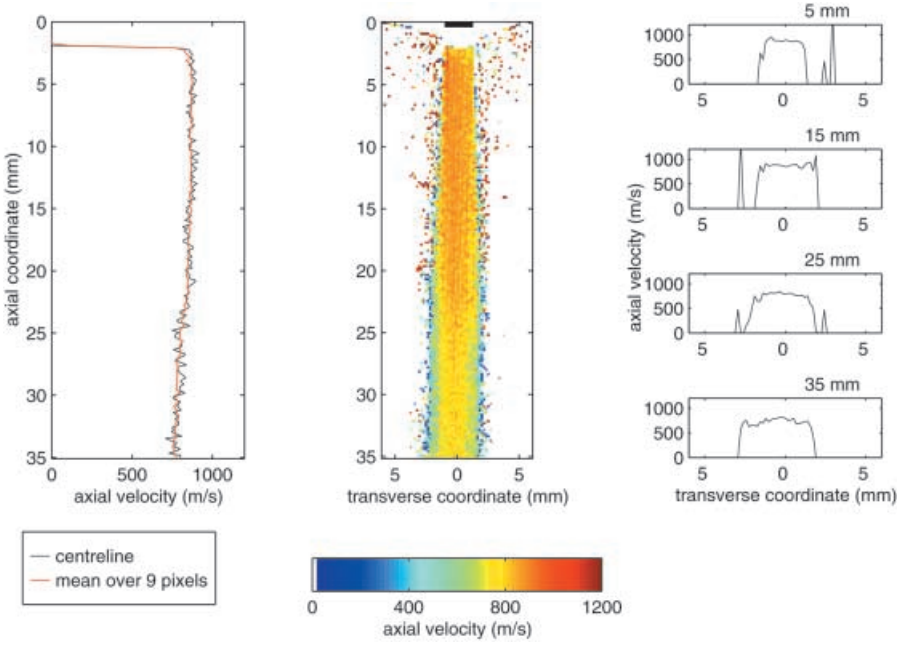

Fig. 10. A colourmap representation of the axial velocity field, an axial profile on the centreline, and profiles at various transverse sections, measured for a payload of 3.0 mg of 15.5 μm polymer microspheres, delivered from a device with a Mach 2.5 contoured nozzle. The bar at the top of the image indicates the position and diameter of the nozzle exit

The lower total pressure and velocity significantly reduce the ability of the shock-processed flow to accelerate particles to higher velocities. An oblique shock system may also be responsible for inducing separation within the nozzle, with the effect of reducing the diameter of the particle jet. The strong fluctuations observed in the pressure histories may be due to oscillation of a shock-induced separation structure.

The numerical model is successful in predicting the gradual decay of cylinder and rupture chamber pressure. Although the timings of membrane burst are accurately predicted, the events immediately following rupture are not. This is because flow in that period is not accurately represented by the assumption of quasi-steady mass fluxes. Prediction of the filling of the rupture chamber before the first burst is poor because the finite opening time of the valve has not been considered.

In particular, the pressure drop (measured and computed) from reservoir to rupture chamber is much greater than the pressure drop across the valve due to friction alone. This is because the pressure in the rupture chamber is determined by the integrated history of mass flows carried in and out of the chamber. As the gas flowing from the reservoir stagnates, its total pressure must drop to match the rupture chamber pressure, through shocks and further viscous losses. This is a significant loss mechanism in the system.

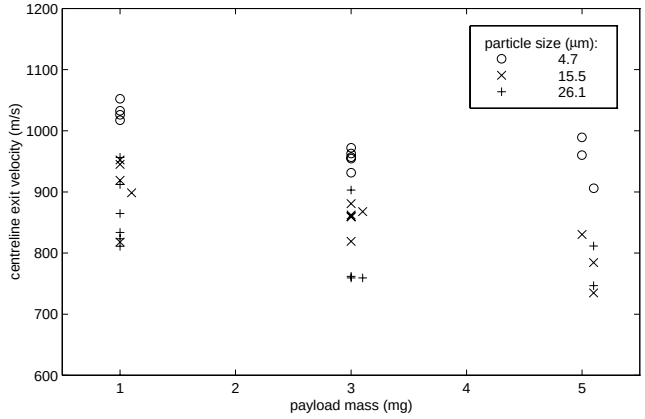

Fig. 11. Measured axial velocities of polymer microspheres, of various sizes and payload masses, on the centreline 5 mm from the exit of the Mach 2.5 nozzle, averaged over a square region measuring 0.9×0.9 mm

4.3 Particle dynamics: contoured nozzle

Measured velocity fields for two typical cases – a 1.0 mg payload of 4.7 μm microspheres, and a 3.0 mg payload of 15.5 μm particles – are presented in Fig. 9 and Fig. 10, respectively, for distances up to 35 mm downstream of the nozzle exit. In drug delivery, the nozzle exit is typically positioned 10 mm from the surface of the skin. Qualitatively, the overall structure of the jet is simple. Velocity is highest on the nozzle centreline and near the exit. It falls off rapidly with distance from the centreline, and decreases gradually with distance downstream of the nozzle exit.

Measured exit velocities for the contoured nozzle, with all tested payloads, are summarised in Fig. 11. Several experimental results were obtained for each test condition. Exit velocity drops as particle diameter is increased. This result reflects the higher drag-to-mass ratio of a smaller particle, and indicates that a significant slip velocity between the gas and particle phases exists at the nozzle exit. Velocity also falls off as payload mass is increased, suggesting that these payload masses are large enough to exert a significant influence on the gas flow. Velocities ranged from 740–810 m/s for 5 mg payloads of 26.1 μm microspheres to 1000–1050 m/s for 4.7 μm spheres. These figures are well above the velocity of 544 m/s estimated for the flow behind the primary shock (in the Mach 3.5 contoured nozzle), suggesting that supersonic nozzle flow, rather than the starting process, is the dominant flow regime for particle acceleration.

4.4 Particle dynamics: conical nozzle

Two typical maps of measured particle velocity in the jet from the conical nozzle, for a 3.0 mg payload of 4.7 μm microspheres and a 5.0 mg payload of 26.1 μm microspheres, respectively, are presented in Fig. 12 and Fig. 13. Some loss of data occurs near the periphery of the jet, where signal in the DGV images is lower because of reduced particle number density and illumination intensity in that region. This difficulty arises only with the conical nozzle because the particle payload (which acts as the light scattering medium for velocimetry purposes) is distributed more sparsely than with the smaller contoured nozzles. Thus, the apparent boundaries of the jet in Figs. 12 and 13 actually represent the threshold of adequate optical signal for velocity measurement.

The typical peak velocities, between 400 and 500 m/s, are substantially less than the velocities of particles delivered with a contoured nozzle. The jet structure is straightforward, with a gradual decay of velocity along the centreline. The transverse distribution of axial velocity in each case is considerably less uniform than in the case of the Mach 2.5 contoured nozzle. This is consistent with the existence of separated flow downstream of a shock system in the conical nozzle.

A summary of the measured exit velocities, in one to four experiments on each of three payload masses and particle types, is shown in Fig. 14. Values range from 310–505 m/s. No systematic dependence of velocity on particle size or payload mass is evident. This suggests that in this time-integrated view of the flowfield, the majority of particles exit the device at or near the gas velocity. The measured particle velocities are comparable with the 345 m/s estimated on the basis of static pressure measurements for gas flow behind the starting shock wave. Furthermore, the particle velocities are much lower than the 1700 m/s gas velocity expected for correctly expanded isentropic flow, confirming that quasi-steady supersonic flow is certainly not involved in particle acceleration. These findings indicate that the starting transient may play a role in particle acceleration to the exit of this nozzle. However, acceleration of particles in the quasi-steady supersonic/shock-processed flow (with Mach number profile as shown in Fig. 8) is equally likely on the basis of these results, and both flow regimes may be important.

5 Conclusions

Measurements and theoretical modelling of gas flow inside the prototype dermal powder delivery device variants investigated show that flow in the nozzle is initiated by an unsteady shock wave, immediately followed by an unsteady expansion. This starting process gives way in under 1 ms to a slowly varying flow-field, which in the case of the contoured nozzle entails supersonic flow throughout the divergent section of the nozzle. DGV measurements of the velocity fields of various payloads delivered by the contoured nozzle show a sensitivity to payload mass and particle size, indicating that particles lag the gas velocity at exit. The smallest particles tested, however, at measured velocities of up to 1050 m/s, approach the isentropic exit gas velocity to within 15%. These observations suggest that quasi-steady supersonic flow, rather than the unsteady starting process, is the primary mechanism determining particle delivery velocity for this device.

In the conical nozzle, which has a larger exit area ratio, supersonic flow at the exit plane is not expected at typ-

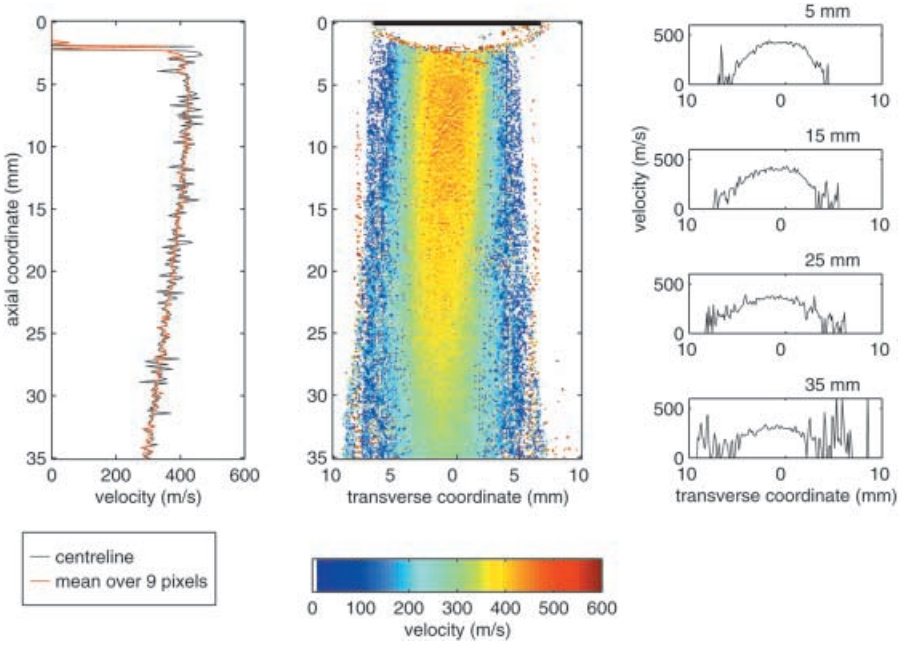

Fig. 12. A colourmap representation of the axial velocity field, an axial profile on the centreline, and profiles at various transverse sections, measured for a payload of 3.0 mg of 4.7 μm polymer microspheres, delivered from a device with a conical nozzle. The bar at the top of the image indicates the position and diameter of the nozzle exit

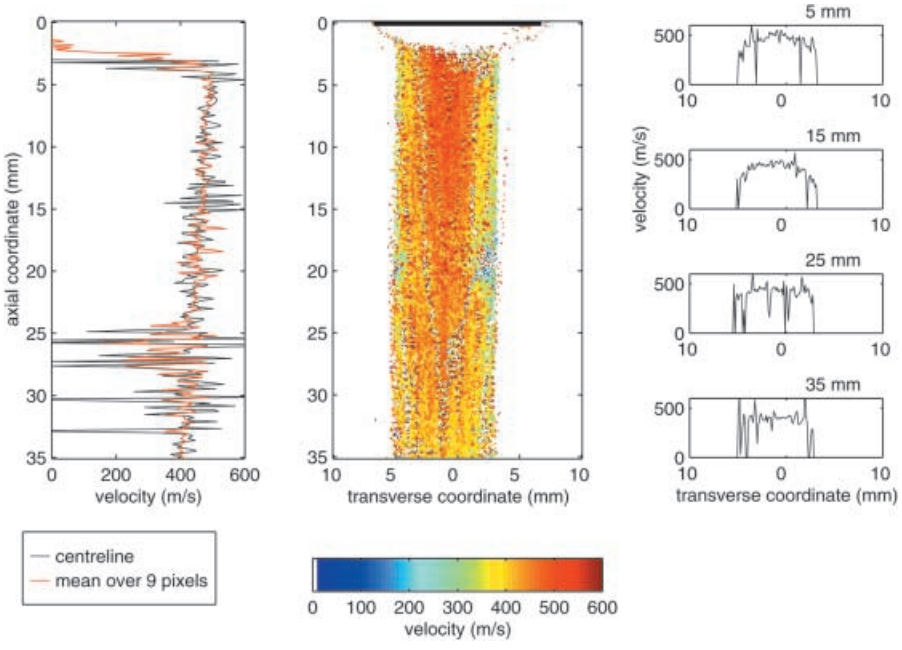

Fig. 13. A colourmap representation of the axial velocity field, an axial profile on the centreline, and profiles at various transverse sections, measured for a payload of 5.0 mg of 26.1 μm polymer microspheres, delivered from a device with a conical nozzle. The bar at the top of the image indicates the position and diameter of the nozzle exit

ical operating conditions. This has been confirmed with static and Pitot pressure measurements, which show that a system of oblique shocks are established in the nozzle approximately 250 μs after the onset of flow. A numerical model of the quasi-steady flow of stored gas from the reservoir system has been developed, and its predictions show excellent agreement with measurements of the decaying pressure in the cylinder and rupture chamber in all but the earliest stages of flow, when the rupture chamber acts as the driver section of a shock tube.

The velocity of particles delivered by the conical nozzle was measured at 310–505 m/s, and was found to be independent of the particle size and payload mass. This suggests that particles have attained gas velocity when they exit the device. The magnitude of the velocity is consistent with acceleration of the particles in the unsteady flow structures of the starting process. There may also be particle acceleration in the quasi-steady supersonic/shock-processed flow. The conical nozzle delivered particles over a relatively large target, offering potential advantages.

In the case of the contoured nozzle, the relatively high velocities observed for the smallest particles are due to the use of helium, with its high speed of sound. However, the larger particles tested do not attain such high velocities, and it is to be expected that particles still larger than those used here will be delivered at progressively lower velocities. In such cases, particle velocities might be maximised by selection of a different gas. Since the accelerating

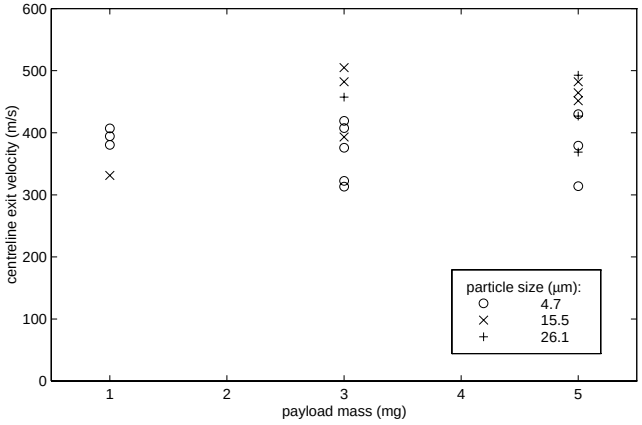

Fig. 14. Measured velocities of polymer microspheres, of various sizes and payload masses, on the centreline 5 mm from the exit of the conical nozzle, averaged over a rectangular region measuring 2.3 (transverse) × 1.1 mm (longitudinal)

force (i.e. the drag) on a particle immersed in a gas flow is proportional to both the gas density and the square of the slip velocity, a gas with a higher density and lower speed of sound could, in principle, yield greater particle acceleration and make more effective use of the energy available in the system.

Future publications will describe two areas of subsequent work on the fluid dynamics of powder injection technology. One area involves the use of time-resolved DGV and schlieren videography to build a more complete picture of the functioning of the first-generation devices described here. Preliminary reports of this work have been published by Quinlan et al. (1999) and Kendall et al. (1999). The second body of research to be described in further publications is oriented towards the development of a family of prototypes which use simple and uniform gas flows to deliver particles with narrower velocity distributions.

Acknowledgements. The authors acknowledge the support of PowderJect Pharmaceuticals plc. DGV research was supported by the Engineering and Physical Sciences Research Council under grant GR/JS4307.

References

Ainsworth RW, Thorpe SJ, Manners RJ (1997) A new approach to flow-field measurement – a view of Doppler global velocimetry techniques. J Heat and Fluid Flow 18:116–130

Amann HO (1969) Experimental study of the starting process in a reflection nozzle. Phys Fluids 12 I:150–153

Bellhouse BJ, Sarphie DF, Greenford CJ (1994) Needle-less syringe using supersonic gas flow for particle delivery. International patent WO94 24263

Bellhouse BJ, Quinlan NJ, Ainsworth RW (1997) Needle-less delivery of drugs, in dry powder form, using shock waves and supersonic flow. In: Houwing AFP (ed) Shock Waves, The Australian National University, Canberra, Australia, pp 51–56

Burkoth TL, Bellhouse BJ, Hewson G, Longridge DJ, Muddle AG, Sarphie DF (1999) Transdermal and transmucosal powdered drug delivery. Critical Reviews in Therapeutic Drug Carrier Systems 16:331–384

Kendall MAF, Quinlan NJ, Thorpe SJ, Ainsworth RW, Bellhouse BJ (1999) The gas-particle dynamics of a high-speed needle-free drug delivery system. In: Ball GJ, Hillier R, Roberts GT (eds) Shock Waves, University of Southampton, UK, pp 605–610

Kendall MAF, Wrighton Smith PJ, Bellhouse BJ (2000) Transdermal ballistic delivery of micro-particles: investigation into skin penetration. World Congress of Medical Physics and Biomedical Engineering, Chicago, IEEE 0-7803-6568-6/00

Meyers JF (1995) Development of Doppler global velocimetry as a flow diagnostics tool. Measurement Sci Tech 6:769–783

Quinlan NJ (1999) Gas and particle dynamics in transdermal powdered drug delivery. D. Phil. thesis, Department of Engineering Science, University of Oxford, UK

Quinlan NJ, Ainsworth RW, Bellhouse BJ, Manners RJ, Thorpe SJ (1997) Application of Doppler global velocimetry to supersonic gas-particle flows in drug delivery. In: Ruck B, Leder A, Dopheide D (eds) Laser Anemometry Advances and Applications, GALA e.V., Karlsruhe, Germany, pp 629–636

Quinlan NJ, Thorpe SJ, Ainsworth RW (1999) Time-resolved Doppler global velocimetry of gas-particle flows in transdermal powder drug delivery. In: Cenedese A, Pietrogiacomi D (eds) Laser Anemometry Advances and Applications, University of Rome, Italy, pp 483–490

Smith CE (1966) The starting process in a hypersonic nozzle. J Fluid Mech 24:625–640

Thorpe SJ, Ainsworth RW, Manners, RJ (1996) Time-averaged free-jet measurements using Doppler global velocimetry. ASME Symposium on Laser Anemometry and Experimental and Numerical Flow Visualisation, San Diego, USA